Molecular Diversity (2026) 30:5227–5245
https://doi.org/10.1007/s11030-025-11418-w

ORIGINAL ARTICLE

Design, synthesis, characterization, computational analysis, structure-activity relationship, and investigation of the anticancer potential of novel dibromodibenzoazepine-based hybrid structures

Azza Allıto[1] · Alper Onder[2] · Ferah Comert Onder[3] · Musa Erdoğan[4,5]

Received: 20 July 2025 / Accepted: 18 November 2025 / Published online: 3 December 2025
© The Author(s), under exclusive licence to Springer Nature Switzerland AG 2025

Abstract

In this study, ten novel dibromodibenzoazepine-substituted triazole hybrid compounds (**AZ1–AZ10**) were designed via a molecular hybridization approach and synthesized using click chemistry methodology. In the synthesis, the dibromodibenzoazepine derivative (**12**) was initially synthesized via bromination. Subsequent propargylation yielded the key intermediate, dibromodibenzoazepine-propargyl derivative (**13**). The Cu (I)-catalyzed azide-alkyne cycloaddition (CuAAC) reaction of propargyl derivative (**13**) with various substituted azide derivatives afforded the target hybrid compounds in high yields. The structures of these compounds were characterized using various spectroscopic techniques, including ^{1}H NMR, ^{13}C NMR, and MS. Among the synthesized compounds, **AZ9** was determined to have the highest cytotoxicity on breast and colon cancer cell lines, including BT20, MCF7, MDA-MB-231, and HT29 with the IC_{50} values of 0.54 ± 0.09 µM, 1.83 ± 0.87 µM, 3.88 ± 0.15 µM, and 5.31 ± 0.38 µM, respectively. In addition, **AZ8** showed the cytotoxicity on BT20 and HT29 cells below 10 µM. The cytotoxicity of **AZ10** in studied cancer cell lines was calculated below 20 µM. The compounds were investigated by computational analysis including molecular docking, molecular dynamics (MD) simulations, Molecular Mechanics with Generalized Born and Surface Area Solvation (MM/GBSA), and ADME predictions. As a result, **AZ8-AZ10** may be promising anticancer agents targeting SphK1 and CDK6 to provide new perspectives for the design and development of novel click products.

Keywords Dibenzoazepine · Triazole · Click chemistry · Anticancer · MD simulation

Introduction

Cancer is a major public health problem worldwide due to dramatically increasing the number of new cases [1]. Due to limitations in current therapies, the lack of the specificity of therapeutic agents, and drug resistance, various strategies such as immunotherapy and gene therapy have been developed for many years [2–4]. Thus, the importance of developing new anticancer agents for the effective treatment of various types of cancer is increasing day by day [5].

Estimates show that the number of new cancer cases will reach 35 million by 2050 [6]. GLOBOCAN stated that there were approximately 1.5 million people in 185 countries with breast and colon cancer in 2022. For this reason, the research on the treatment of breast and colon cancers has gained importance [6, 7].

✉ Musa Erdoğan
musaerdogan0@gmail.com; musa.erdogan@kafkas.edu.tr

1 Department of Interdisciplinary Biotechnology, Institute of Natural and Applied Sciences, Kafkas University, Kars, Türkiye

2 Natural Products and Drug Research Laboratory, Department of Chemistry, Faculty of Science, Çanakkale Onsekiz Mart University, 17020 Çanakkale, Türkiye

3 Department of Medical Biology, Faculty of Medicine, Çanakkale Onsekiz Mart University, 17020 Çanakkale, Türkiye

4 Department of Food Engineering, Faculty of Engineering and Architecture, Kafkas University, Kars, Türkiye

5 Department of Industrial Engineering, Faculty of Engineering and Architecture, Kafkas University, Kars, Türkiye

As is known the development of cancer drugs is time-consuming and costly [8, 9]. In recent years, drug development studies have been intensively carried out by computational approaches for important target-oriented cancer research [10, 11]. Therefore, the interactions between receptors and ligands are successfully elucidated with molecular docking and molecular dynamic (MD) simulation studies towards important drug targets to determine new scaffolds and pharmacophore groups [12]. Especially in the field of drug design and development, heterocyclic compounds containing nitrogen atoms play a crucial role in medicinal chemistry due to their diverse biological activities [13, 14]. Among these, 5 H-dibenzo[b, f]azepine (also known as iminostilbene) and its derivatives have recently garnered attention not only due to their well-established neurological and biological activities [15–17] but also for their potential applications in cancer treatment [18, 19]. For instance, iminodibenzyl and its derivatives have been shown to interfere with cyclooxygenase-2 (COX-2) activity, which is known to promote cancer cell proliferation and survival. Beyond COX-2 inhibition, dibenzoazepine derivatives have also been reported to affect other critical targets in cancer biology, such as histone deacetylases (HDACs) and metabolic enzymes involved in cellular proliferation. By altering gene expression and epigenetic regulation, these compounds can promote apoptosis and disrupt the survival mechanisms of tumor cells [20].

Another promising approach in cancer drug design involves the structural modification of 5 H-dibenzo[b, f]azepine derivatives to enhance their selectivity and potency. 1,2,3-Triazoles are nitrogenous heterocycles characterized by the presence of three nitrogen atoms inside the ring structure. 1,2,3-Triazoles are stable molecules that engage with biological targets through the formation of intermolecular hydrogen bonds, making them significant scaffolds in drug discovery [21].

Figure 1 illustrates anticancer medicines that incorporate 1,2,3-triazole scaffolds in their architectures [22, 23]. Derivatives of 1,2,3-triazole have been documented to exhibit various pharmacological activities, including, antibacterial, antifungal, antitubercular, anti-diabetic, anti-inflammatory, anti-microbial, anti-HIV, and antiviral actions [24–30].

Hybrid molecules incorporating azepine cores with other bioactive moieties, such as triazole rings, have been synthesized to improve their interaction with cancer-related enzymes. These hybrid compounds have demonstrated increased anticancer activity, particularly in triple-negative breast cancer (TNBC) models, where treatment options remain limited [19, 31].

Result and discussion

Chemistry

The synthesis of the click products commenced with the preparation of the propargyl and azide derivatives. Initially, the synthesis of the ten different substituted azide derivatives **1–10** required for the click reaction was carried out using methods previously reported in our earlier work [32]. Then, the dibromoazepine derivative **13** was synthesized. Under a nitrogen atmosphere, this compound was treated with KO*t*-Bu in distilled DMF at 0 °C for 10 min. Subsequently, propargyl bromide was added to the reaction mixture, leading to the formation of intermediate **13** in high yield (Scheme 1). The progress of the reaction was monitored by TLC and ^{1}H NMR analysis.

Upon examining the ^{1}H NMR spectrum of dibromoazepine derivative **12**, it is observed that the -NH proton of the azepine ring resonates as a broad singlet at 5.96 ppm (bs, 1 H, -NH). The disappearance of the -NH proton signal in the ^{1}H NMR spectrum of propargylated product **13** confirms the formation of the *N*-propargylated compound. The presence of the propargyl moiety in compound **13** is confirmed by the appearance of a doublet at 4.38 ppm (d, J = 2.4 Hz, 2 H) corresponding to the -CH_2- protons and a triplet at 2.39 ppm (t, J = 2.4 Hz, 1 H) corresponding to the acetylenic proton. In the final step, target products were synthesized through the CuAAC reaction between various azide derivatives and propargyl derivatives. $CuSO_4$ and CuI, along with (+) Sodium *L*-ascorbate, were used as a catalyst in the click reaction. A catalytic amount of NEt₃ was added to the reaction medium. All click reactions were conducted in a THF/H_2O (2:1, v/v, mL) solvent mixture at 70 °C for 12 h (Scheme 2). The click products were purified using silica gel column chromatography. The molecular structures of the isolated products were elucidated using various spectroscopic characterization methods, including ^{1}H NMR, ^{13}C NMR, and HRMS.

In Fig. 2, the common skeletal structure of the synthesized click products is given. In the synthesis of click products, the propargyl unit, which serves as a key structure, was analyzed by comparing the ^{1}H and ^{13}C NMR spectra of the click products with the starting compound **13**. It was observed that the signals in the aliphatic region corresponding to the propargyl group in compound **13** disappeared, while the C-H signal of the triazole ring and other skeletal signals appeared.

In the ^{1}H NMR spectra, the four identical H1 protons of the symmetric dibromodibenzoazepine ring resonated as a singlet in the range of 3.13–3.06 ppm. The aromatic H2, H3, and H4 protons of the dibenzoazepine ring primarily gave multiplet signals in the range of 7.5–6.9 ppm

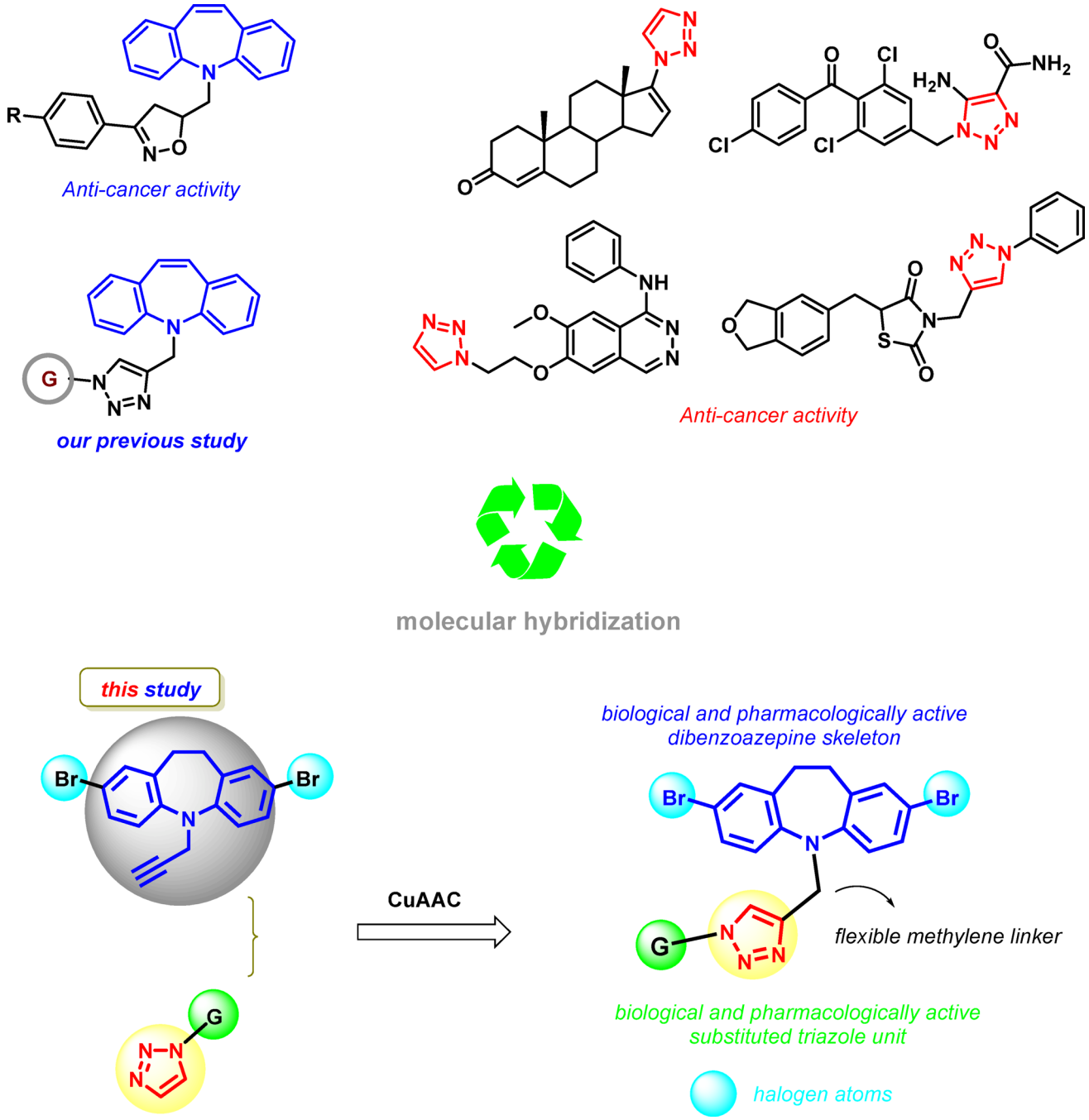

Fig. 1 Design of dibromodibenzoazepine substituted-triazole derivatives

(Fig. 2). The two identical H5 protons of the methylene (-CH_2-) bridge linking the dibenzoazepine and triazole rings appeared as a singlet in the expected region (5.13–4.96 ppm). The one H6 proton from the triazole ring in the common dibenzoazepine-triazole hybrid part resonated as a singlet in the 8.93–7.97 ppm range. The characteristic signals of the skeletons derived from the azide unit incorporated into the hybrid structure (the part of the triazole ring in Fig. 7, excluding the common skeleton) appeared in the expected regions of the ^{1}H NMR spectrum. For example, the identical protons in the benzylic positions of the **AZ1** product resonated as singlets at 5.50 ppm. The aromatic ring protons of the **AZ2** product split into separate doublets with a coupling constant of $J = 8.8$ Hz, interacting at 7.88 ppm (2 H) and 7.63 ppm (2 H), respectively. In the **AZ3** compound, the protons located on either side of the nitrogen atom in the pyridyl skeleton appeared at lower fields due to the inductive effect

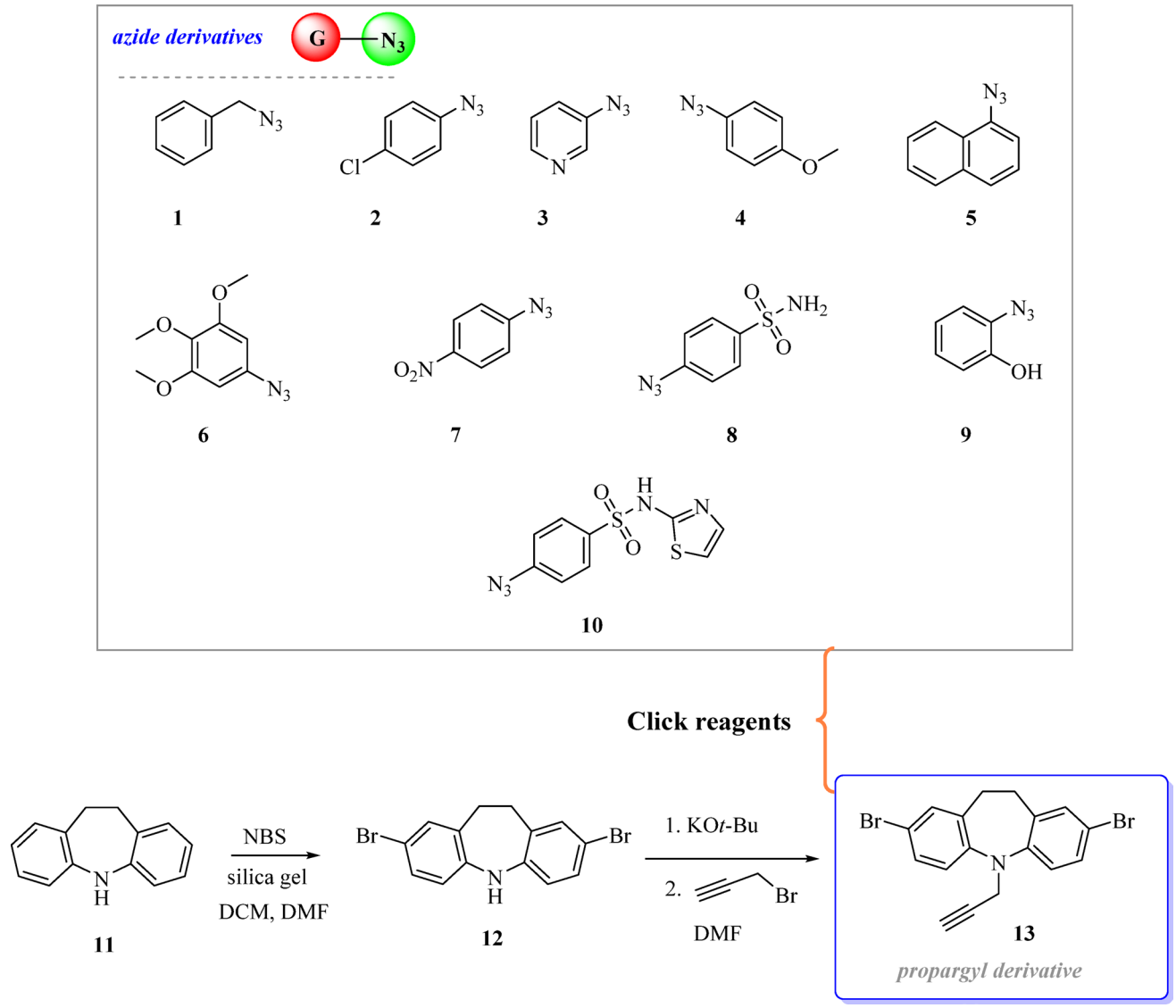

Scheme 1 Synthesis of propargyl derivative **3** and azide derivatives **4–13** used in click reaction

of the nitrogen atom, with lower coupling constants compared to the other aromatic ring protons. These protons resonated at 9.09 ppm (s, J = 2.1 Hz, 1 H) and 8.66 ppm (d, J = 8.3, 4.6 Hz, 1 H), respectively. The aromatic ring protons of the **AZ4** product split into doublets with a coupling constant of J = 9.0 Hz, interacting at 7.73 ppm (2 H) and 7.04 ppm (2 H), respectively. The -OMe protons at the para position of this ring appeared as a singlet at 3.80 ppm (3 H). For the **AZ5** molecule, the aromatic ring protons of the naphthalene unit resonated in the range of 8.16–6.63 ppm. For the **AZ6** molecule, the two identical protons in the symmetric aromatic ring attached to the triazole ring appeared as a singlet at 7.12 ppm. The two identical -OMe protons (6 H) in the meta position of the triazole ring resonated as a singlet at 3.85 ppm, while the -OMe protons at the para position gave a singlet signal at 3.68 ppm. The aromatic ring protons of the **AZ7** product split into doublets with a coupling constant of J = 9.1 Hz, interacting at 8.41 ppm (2 H) and 8.16 ppm (2 H), respectively. In the **AZ8** product, the aromatic ring protons split into doublets with a coupling constant of J = 8.7 Hz, interacting at 8.06 ppm (2 H) and 7.98 ppm (2 H), respectively. The -NH_2 protons (2 H) in the sulfonamide unit of this structure resonated as a broad singlet at 7.53 ppm. In the **AZ9** molecule, the -OH signal in the ortho position of the triazole ring appeared as a broad singlet at 10.51 ppm, while the other aromatic ring protons resonated in the aromatic region between 7.54 and 6.94 ppm. For the **AZ10** molecule, the characteristic –NH- signal in the sulfothiazole skeleton attached to the triazole ring resonated as a broad singlet at 12.87 ppm, as expected. In the ^{13}C NMR spectra, signals corresponding

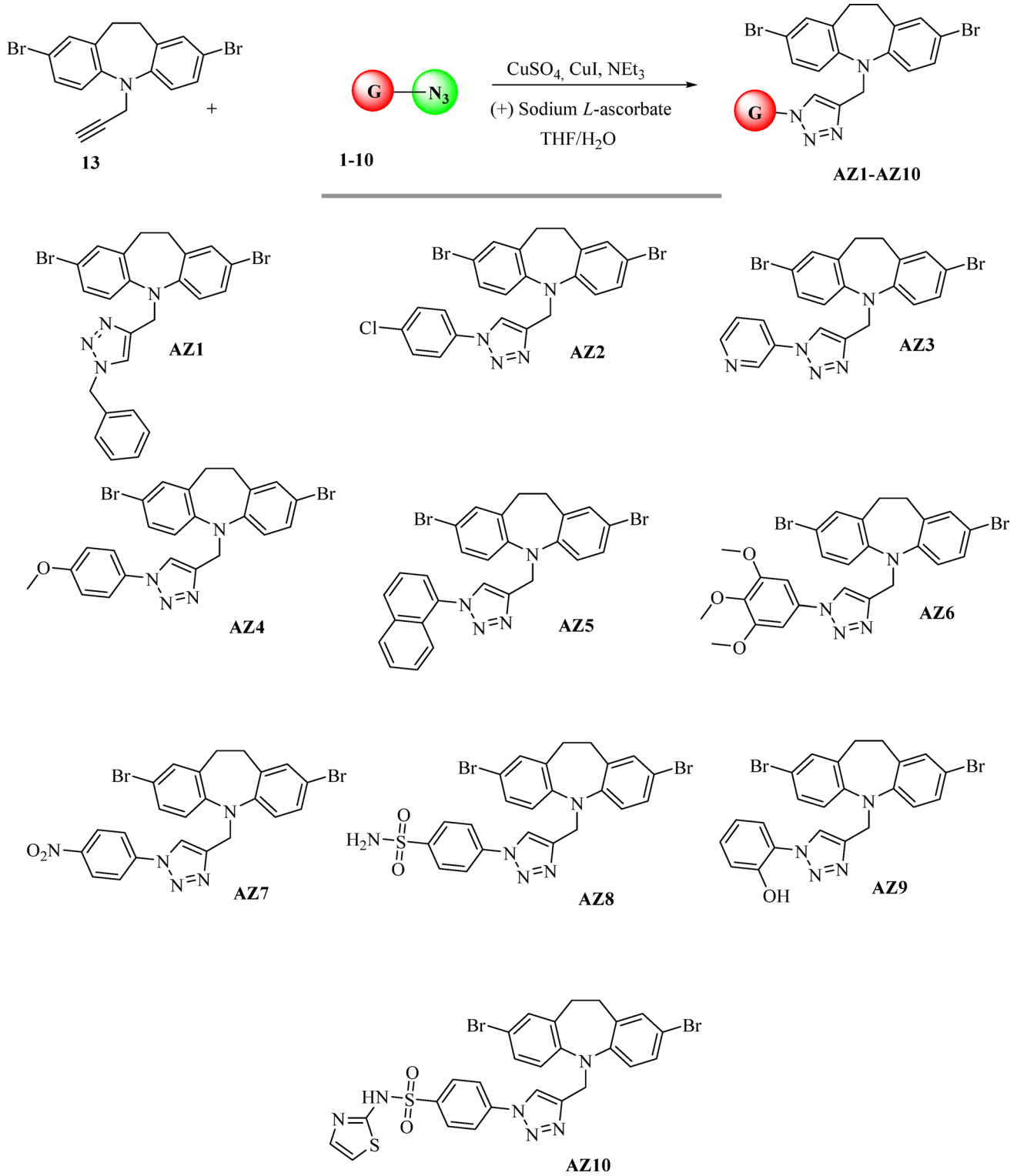

Scheme 2 Synthesis procedure of Click products **AZ1-AZ10**

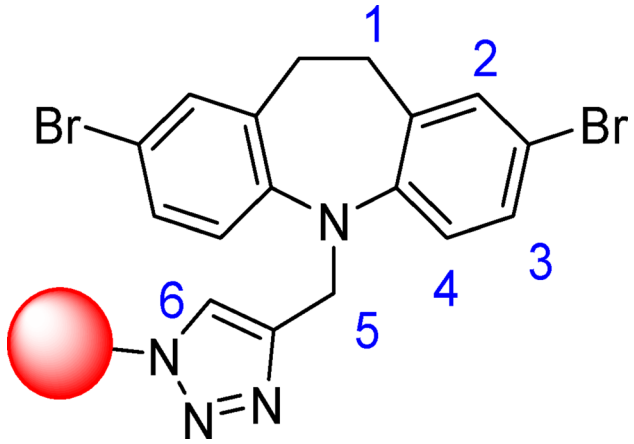

Fig. 2 Common skeleton structure of the synthesized click products

Table 1 IC_{50} values of the synthesized click products in various cancer cell lines

Compounds	IC_{50} (μM)			
	MDA-MB-231	BT20	MCF7	HT29
AZ1	>100	>100	>100	>100
AZ2	>100	>100	>100	>100
AZ3	>100	>100	>100	>50
AZ4	35.65 ± 11.84	4.85 ± 0.92	7.62 ± 1.58	26.63 ± 4.40
AZ5	85.06 ± 10.93	>100	>100	>100
AZ6	>100	>100	>100	>100
AZ7	>20	8.78 ± 2.60	>20	>100
AZ8	11.05 ± 0.96	7.62 ± 0.42	12.51 ± 1.18	8.25 ± 0.93
AZ9	3.88 ± 0.15	0.54 ± 0.09	1.83 ± 0.87	5.31 ± 0.38
AZ10	13.56 ± 1.1	16.48 ± 2.88	19.88 ± 3.07	19.10 ± 3.10

± indicates standard deviation (SD)

to the number of carbon atoms in all click products were observed. Furthermore, the signals for the carbons in the aliphatic and aromatic regions, along with their chemical shift values, are in good agreement with the structures of the molecules. The experimentally obtained mass values from the analysis of all click products are in excellent agreement with the theoretically calculated mass values.

Anticancer activity

To investigate the anticancer effects of the synthesized click products, various human cancer cell lines, including TNBC (MDA-MB-231 and BT20) and ER+ (MCF7) and colon (HT29) were used (Table 1). In the cytotoxicity analysis, the 96 h treatments in the increasing concentrations of the compounds were carried out. The compounds (**AZ8-AZ10**) decreased the cell viability between 0.5 and 20 μM concentrations. Accordingly, among the synthesized compounds, **AZ9** was determined to have the highest cytotoxicity with the IC_{50} value of 0.54 ± 0.09 μM on TNBC BT20 cells. Besides, **AZ9** showed the cytotoxicity on MCF7, MDA-MB-231, and HT29 cell lines with the IC_{50} values of 1.83 ± 0.87 μM, 3.88 ± 0.15 μM, and 5.31 ± 0.38 μM, respectively. In the BT20 cell line, the IC_{50} values of **AZ4**, **AZ7**, and **AZ8** were calculated to be 4.85 ± 0.92 μM, 7.62 ± 0.42 μM, and 8.78 ± 2.60 μM, respectively. In addition, **AZ10** showed the cytotoxicity on BT20 cells at 16.48 ± 2.88 μM. The cytotoxicity of **AZ8** and **AZ10** on MDA-MB-231 cells was calculated with the IC_{50} values of 11.05 ± 0.96 μM and 13.56 ± 1.1 μM, respectively. In the HT29 cell line, **AZ8** showed cytotoxic effect below 10 μM like **AZ9**. The IC_{50} values of **AZ4** and **AZ7** on MDA-MB-231 cells were found to be 35.65 ± 11.84 μM and 85.06 ± 10.93 μM, respectively. Although **AZ8-AZ10** showed anticancer effect at low concentrations in the MDA-MB-231 cell line, the IC_{50} values of **AZ1-AZ3** and **AZ6** were calculated above >100 μM. The IC_{50} values of **AZ4** and **AZ10** on colon cancer cell line were found 26.63 ± 4.40 μM and 19.10 ± 3.10 μM, respectively. **AZ1-AZ3**, **AZ5**, and **AZ6** showed no cytotoxic activity in most cell lines up to 100 μM. Overall, in this study, we focused on two cancer types including four different cancer cell lines. These findings show that **AZ9** has the highly selectivity for the studied cancer cell lines. **AZ8-AZ10** have been determined to be promising anticancer agents.

Computational analysis

Molecular docking

The binding patterns of the synthesized novel triazole-linked click products were determined by the Glide/SP method. For this study, the compounds were analyzed in silico studies against important drug targets such as SphK1 and CDK6 for the first time. Herein, the binding abilities of **AZ1** and **AZ9** among dibromodibenzoazepine-based hybrid structures against SphK1 were calculated to be -8.486 kcal/mol and −7.948 kcal/mol, respectively. In vitro anticancer effective **AZ9** interacted with the key residues in the binding pocket of SphK1. The dibromodibenzoazepine scaffold of **AZ1** interacted with the residues of Met392, Phe259, Leu286, Leu345, and Leu385 to form pi-pi and pi-alkyl interactions. In addition, the interactions, including pi-sigma, pi-pi, and pi-alkyl were observed between the triazole ring and the residues of Ile260, Phe389, and Val263 for **AZ1**. The dibromodibenzoazepine scaffold of **AZ9** interacted with the residues of Phe259, Phe389, Leu345, Leu385, and Leu388, forming pi-sigma and pi-pi interactions. A

conventional hydrogen bond was observed between the hydroxy-substituted phenyl ring of **AZ9** and the residue of Ile260 of SphK1. Although **AZ1** has no anticancer activity at low concentrations, it has the highest binding energy with in silico analysis. Moreover, **AZ1** showed the highest binding pattern against CDK6. It was followed by **AZ6**, **AZ10**, **AZ9**, and **AZ8** with the top docking scores including −7.625 kcal/mol, -7.521 kcal/mol, -7.383 kcal/mol, and −7.314 kcal/mol, respectively. The interactions such as conventional H-bond and alkyl with the residues, including Ala41, Ala162, Asp163, His100, Ile19, Leu152, Lys43, Phe98, Val101, Val27, and Val77 of CDK6 were observed. Consequently, ligand interaction profiles of the most cytotoxic compounds **AZ8** and **AZ9** were shown for important cancer drug targets (Fig. 3). We first reported thein silicoanalysis for a series of dibenzoazepine-substituted triazole hybrids as potential SphK1 and CDK6 inhibitors [19]. Herein, it has been reported that newly designed and synthesized dibromodibenzoazepine-based hybrid compounds may be potential inhibitor candidates for the studied drug targets. Figure 4A, B shows the binding patterns of the compounds in the binding pocket of the protein. In this study, sulfonyl-containing compounds **AZ8** and **AZ10** may be potential inhibitor candidates of CDK6 to be used in vitro analysis. It has been reported that sulfonyl-containing compounds Roniciclib (BAY 1000394) and AZD5438 developed by Bayer and AstraZeneca, respectively, are called as first and second generation pan-CDK inhibitors. Roniciclib showed antiproliferative activity against breast cancer cell lines and inhibited tumor growth [33, 34]. AZD5438 exhibited the inhibition on tumor volume towards colorectal, ovarian, and prostate cancer xenografts [33, 35]. Among the synthesized compounds, sulfonamide-containing compounds displayed strong binding abilities towards SphK1, and interactions were analyzed in detail for the first time [19, 36]. We demonstrated that sulfonamide moiety on hybrid compounds contribute to increase anticancer activity [19, 36]. According to the reported studies with the SphK1 reference inhibitors PF543 and SKI-II, the docking scores were given at values ranging from −8.8 kcal/mol to −9.90 kcal/mol [37, 38]. It was reported that in silico analysis of known inhibitors PF-543 and SKI-II [19, 36, 39, 40]. Therefore, dibromodibenzoazepine-based hybrid compounds could be good inhibitor candidates for targeting SPhK1 and/or CDK6, which are important for cancer therapy.

Molecular dynamics (MD) simulations and molecular mechanics with generalized born and surface area (MM/GBSA)

Among the studied compounds, the top docking poses of the potential compounds (**AZ1**, **AZ8-AZ10**) with the highest binding energy and in vitro anticancer activity were used for MD simulations. Hydrophobic and pi-pi interactions between the residues Phe259 and Phe278 of SphK1 and **AZ1** were observed. Additionally, 2-hydroxy substitution on the phenyl ring of **AZ9** interacted with the residue Thr282 of SphK1 (Fig. 5). Triazole ring and its nitrogen atom of **AZ1** interacted with His100 and Val101 of CDK6, respectively. Two nitrogen atoms on the triazole ring of **AZ10** interacted with Asp163 and Lys43 via water bridges. Moreover, it can be seen in Fig. 6 that the interactions between oxygen atoms of sulfonamide groups of **AZ8** and **AZ10** and the residue Lys147 of CDK6. Overall, these interaction analyses highlight that **AZ1**, **AZ8-AZ10** may show more potency targeting CDK6. In the RMSD plot in Fig. 7A, the average RMSD values of protein Cα for **AZ1** and **AZ9** were calculated to be 2.01 ± 0.40 Å and 1.71 ± 0.17 Å, respectively. The average RMSD values of protein Cα for **AZ1**, **AZ8**, **AZ9**, and **AZ10** were found to be 2.04 ± 0.23, 1.93 ± 0.29, 1.86 ± 0.18, and 2.27 ± 0.21 Å, respectively (Fig. 7B). In Table 2, the binding free energies (ΔG_{bind}) were calculated by the Prime method between −84.06 ± 4.42 kcal/mol and −61.57 ± 2.58 kcal/mol. As seen in Table 2; Fig. 8, the comparative results show that **AZ9** and **AZ10** have the highest binding free energy values targeting SphK1 and CDK6, respectively.

In our previously reported studies, we indicated that the highest average RMSD value was found for a sulfonamide-containing triazole-linked click product [19, 36]. The average RMSD value of the protein Cα for a potential sulfonamide-containing hybrid product (ΔG_{bind} = −78.82 ± 5.82 kcal/mol) was reported to be 1.96 ± 0.34 Å targeting SphK1 [19]. Herein, the average RMSD value for **AZ8** was reported to be 1.93 ± 0.29 Å (ΔG_{bind} = -71.06 ± 5.86 kcal/mol). Based on the reported studies [19, 36], it can be said that the roles of the click products on important cancer drug targets such as SphK1 and CDKs can be evaluated by further in vitro and in vivo analysis.

In silico ADME analysis

In silico ADME (Absorption, Distribution, Metabolism, Elimination) analysis of click products for physicochemical and drug-likeness properties indicate that the predicted octanol/water distribution coefficient were found in the expected ranges for **AZ1** and **AZ2**, and borderline for **AZ4** and **AZ5**. The predicted water/gas distribution

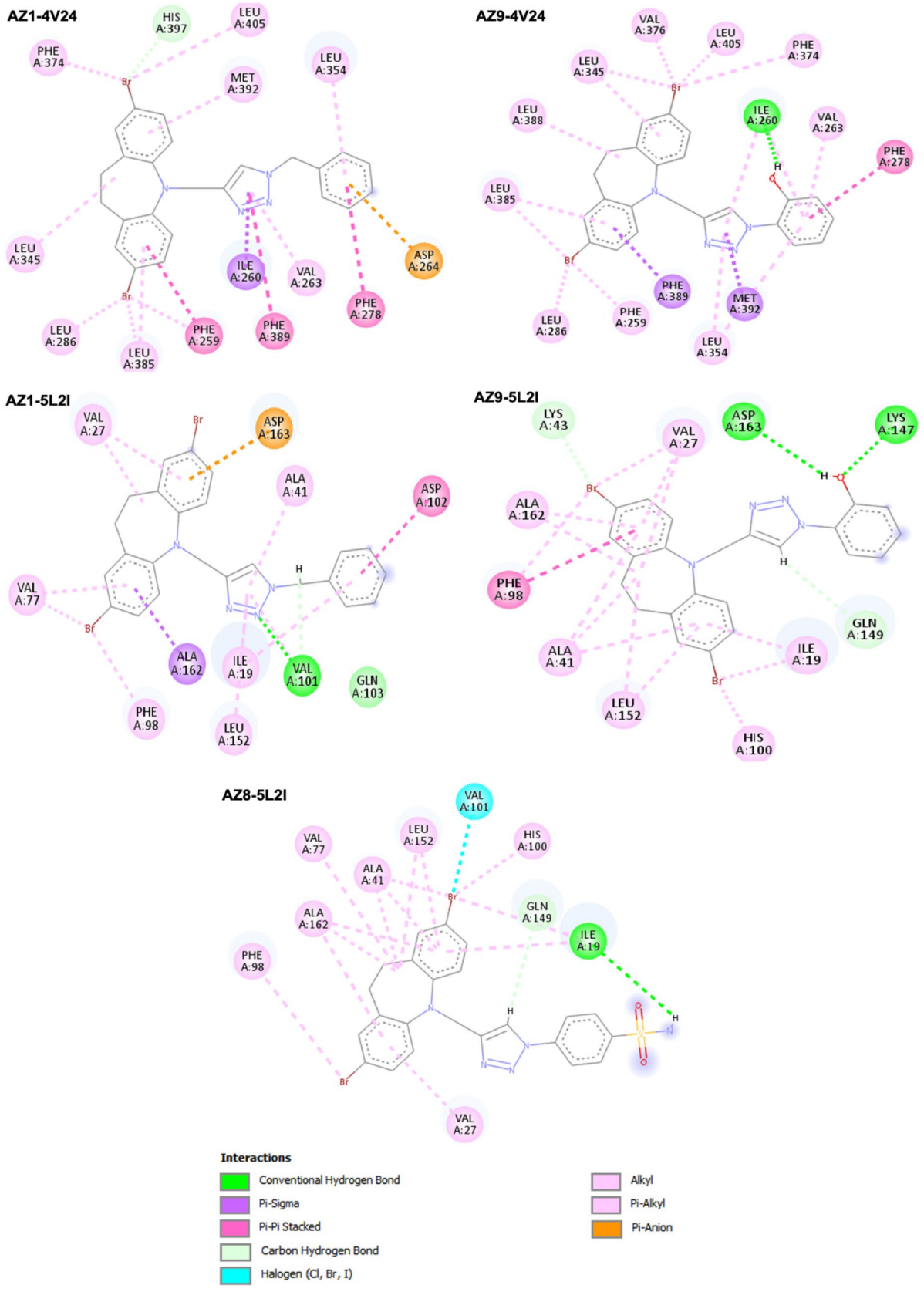

Fig. 3 2D Interaction diagrams of **AZ1**, **AZ8**, and **AZ9** targeting SphK1 and CDK6

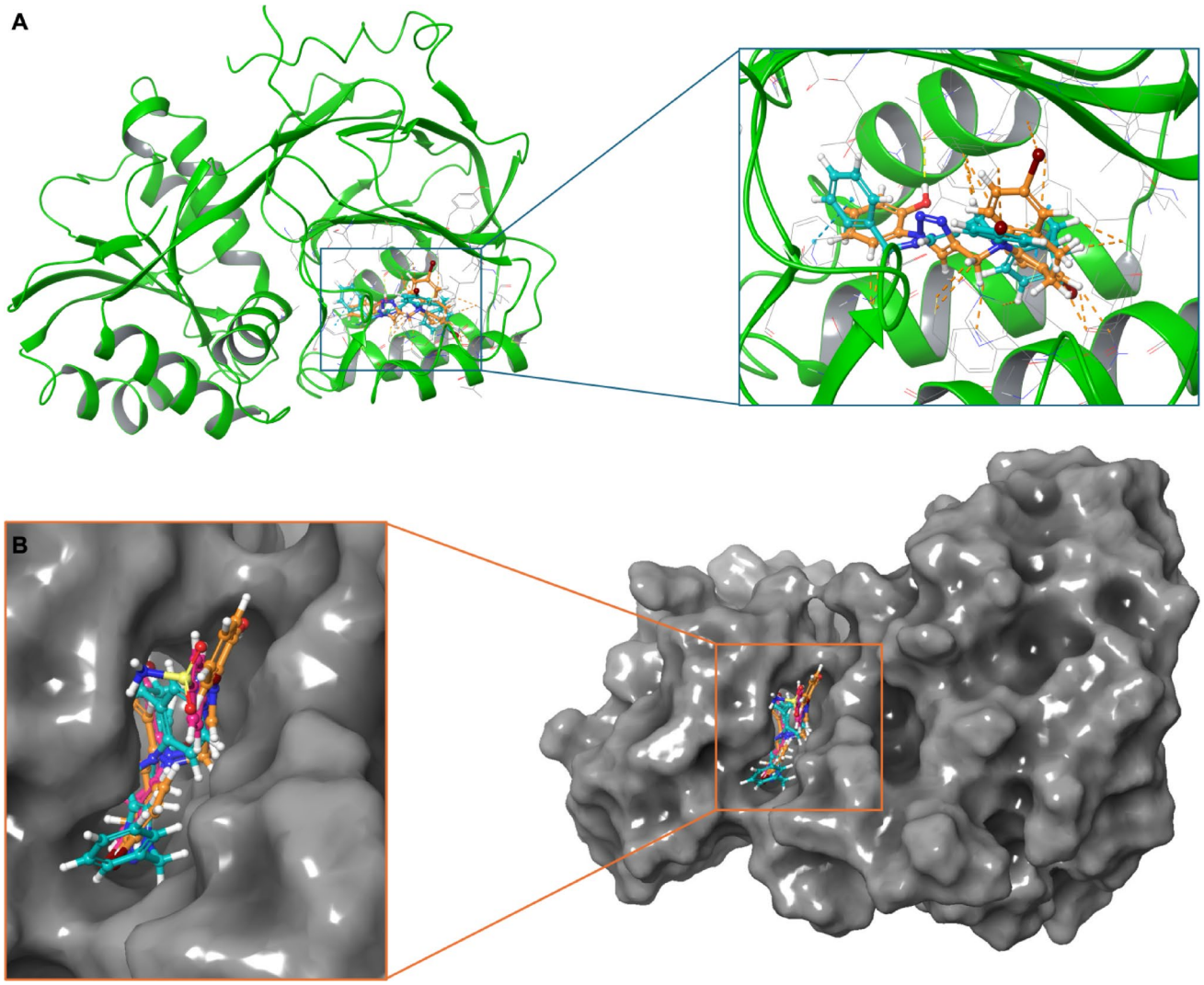

Fig. 4 Binding poses of the compounds **A** SphK1-**AZ1** (blue) and **AZ9** (orange), **B** CDK6-**AZ1** (blue), **AZ8** (pink), **AZ9** (orange)

coefficients were calculated in the expected range for all compounds. The aqueous solubility was not estimated in the expected values. Caco-2 cell permeability was predicted to be very good for the compounds except for **AZ7**, **AZ8**, and **AZ10**. The predictions of brain/blood distribution and skin permeability were found in the expected ranges. The estimated IC_{50} values of the compounds for blockade of HERG K + channels below − 5 may be a concern. The binding to human serum albumin values were predicted to be acceptable except for **AZ5**. Human oral absorption values are low for the compounds. The values of Lipinski's rule of five are acceptable in Table 3 as indicated in the previous studies [19, 41–43].

ADME predictions show that synthesized click products might exhibit low oral absorption. To overcome this restriction, prodrug design could improve lipophilicity, aqueous solubility, and bioavailability [44]. In addition, formulation strategies such as lipid-based systems, nano emulsions may enhance solubility, bioavailability, and intestinal uptake [45, 46].

Structure-activity relationship (SAR)

Synthesized click products were analyzed using in vitro anticancer activity and in silico studies to evaluate their anticancer activities and inhibitor potentials. Among the synthesized compounds, **AZ9** is the most cytotoxic agent on four different human cancer cell lines. The substitution with 2-hydroxyphenyl linked to 1,2,3-triazole ring of **AZ9** increased the anticancer activity in tested various human cancer cell lines. The free hydroxyl group contributed to the formation of a hydrogen bond with carbonyl oxygen of the residue Ile260. A hydrogen bond was observed between the sulfonamide moiety of **AZ8** and the residue Ile19. Moreover, the formation of an intramolecular hydrogen bond

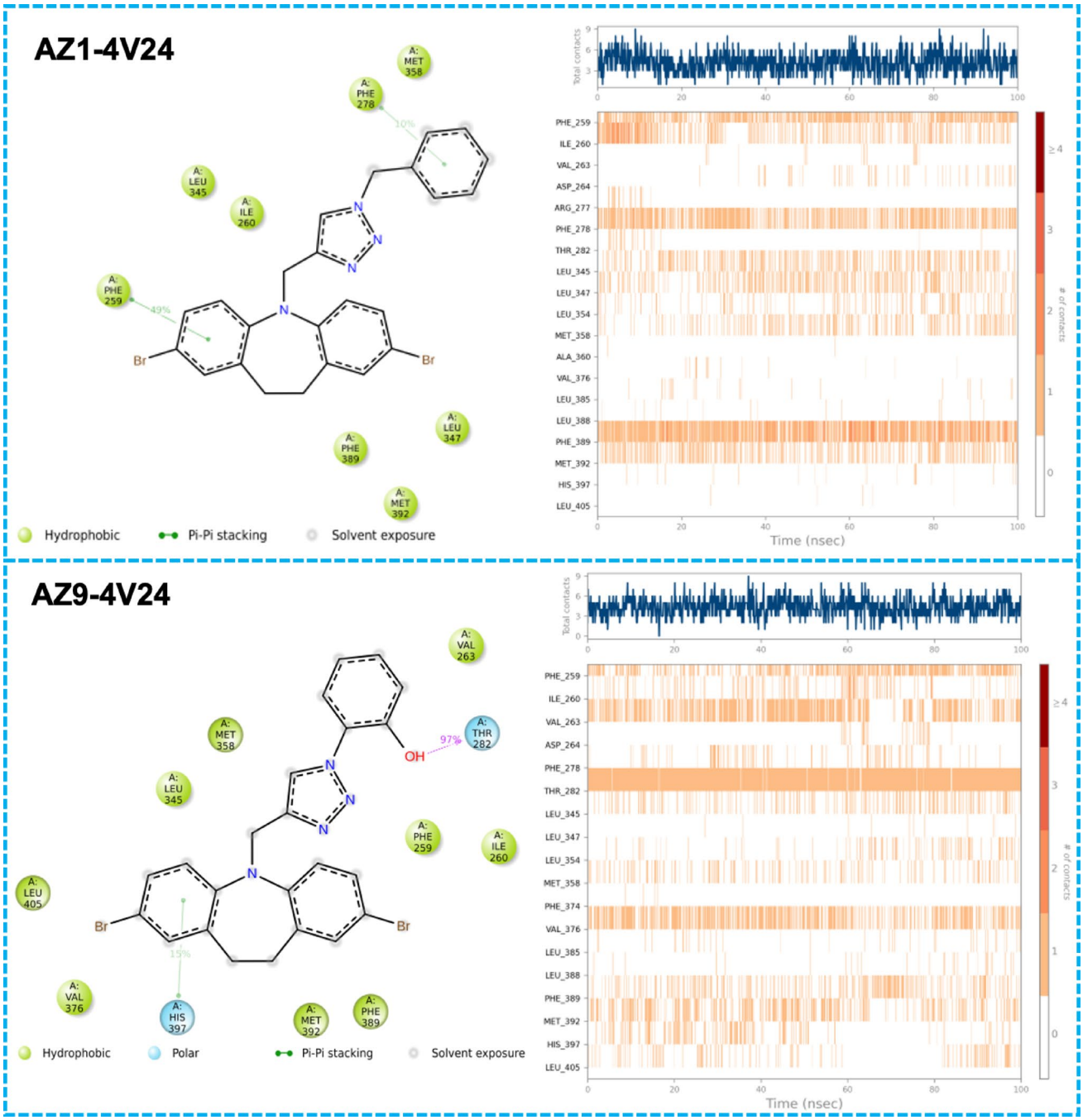

Fig. 5 Interaction diagram and protein-ligand contacts of **AZ1** and **AZ9** against SphK1 throughout the MD simulations

between the -NH of thiazole ring and sulfonyl group of **AZ10** was observed (Fig. 9). It is indicated that these compounds were determined to be highly cytotoxic agents on cancer cell lines. Computational analyses were performed to elucidate the intermolecular interactions towards the potential cancer drug targets such as SphK1 and CDK6, and to determine the stability of the protein-ligand complexes and binding free energies. For **AZ4**, **AZ8**, **AZ9**, and **AZ10**, the substitution of 4-methoxy, sulfonamide, 2-hydroxy, and thiazole-containing sulfonamide on phenyl ring increased the anticancer activity on the studied cancer cell lines. Finally, it can be said that the 10,11-dihydrodibenzoazepine skeleton with dibromo-subsution at positions 2 and 8 may enhances the anticancer activity compared to the dibenzoazepine skeleton [tit19].

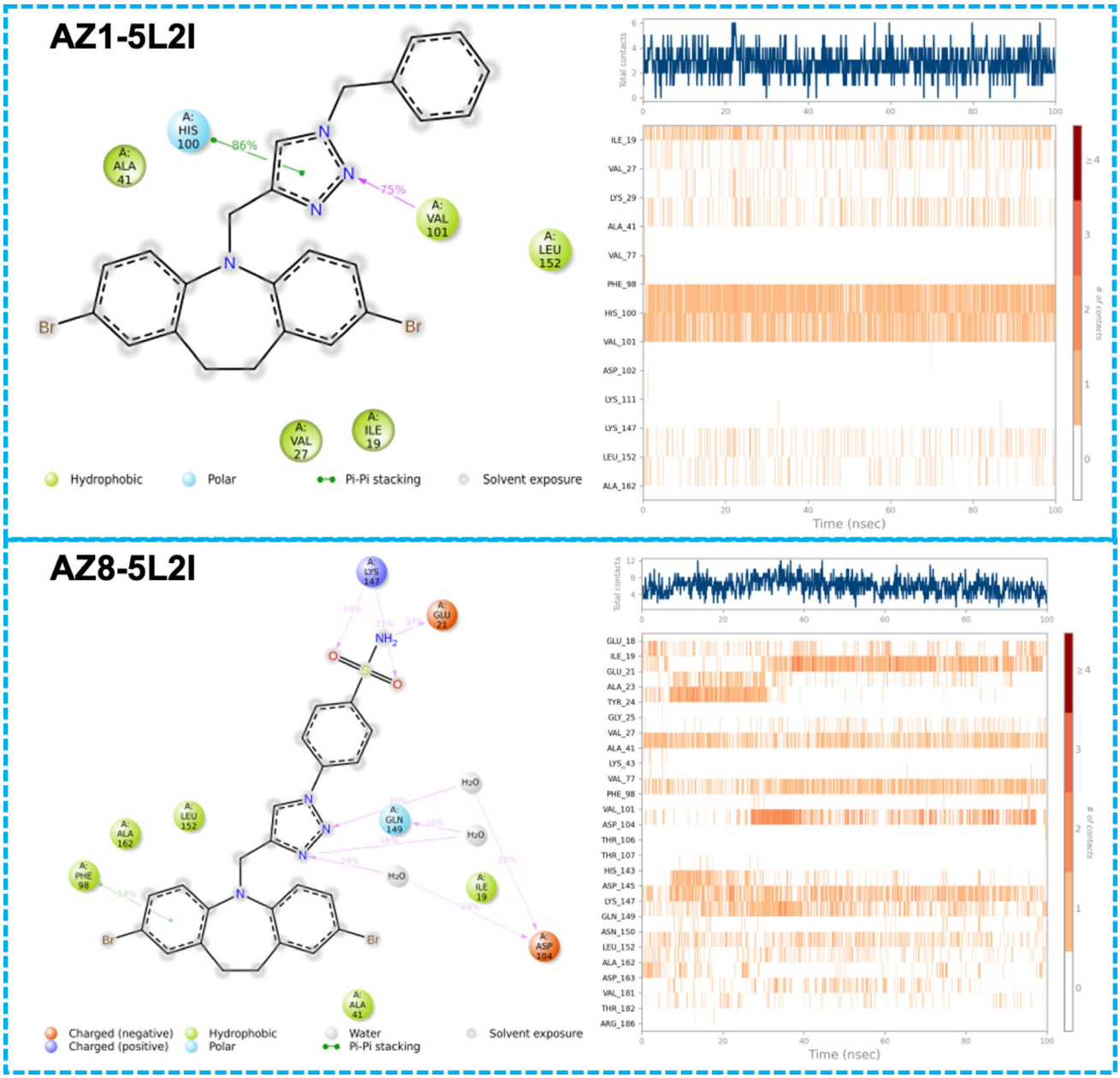

Fig. 6 Interaction diagram and protein-ligand contacts of **AZ1** and **AZ8** against CDK6 throughout the MD simulations

Conclusion

Dibromodibenzoazepine-based triazole hybrids were designed by molecular hybridization approach and synthesized in good yields using click chemistry. **AZ9** was found to be the most potent anticancer agent with its highest cytotoxicity in four different cancer cell lines. It was followed by a sulfonamide-containing **AZ8** and **AZ10**. Moreover, it was determined that synthesized some hybrid compounds could be potential inhibitor candidates of SphK1 and CDK6. These findings were supported by integrated in vitro anticancer activity and in silico analyses in this study for the first time. It is thought that these studied click products may be promising anticancer agents for various cancer types. Overall, in vitro and in vivo studies for these lead compounds can be suggested as future perspectives, and these click products may be used in combination therapies for cancer therapy.

Experimental

All reactions were conducted under an inert nitrogen atmosphere, and we monitored the reaction progress via thin layer chromatography (TLC), utilizing Fluka silica gel

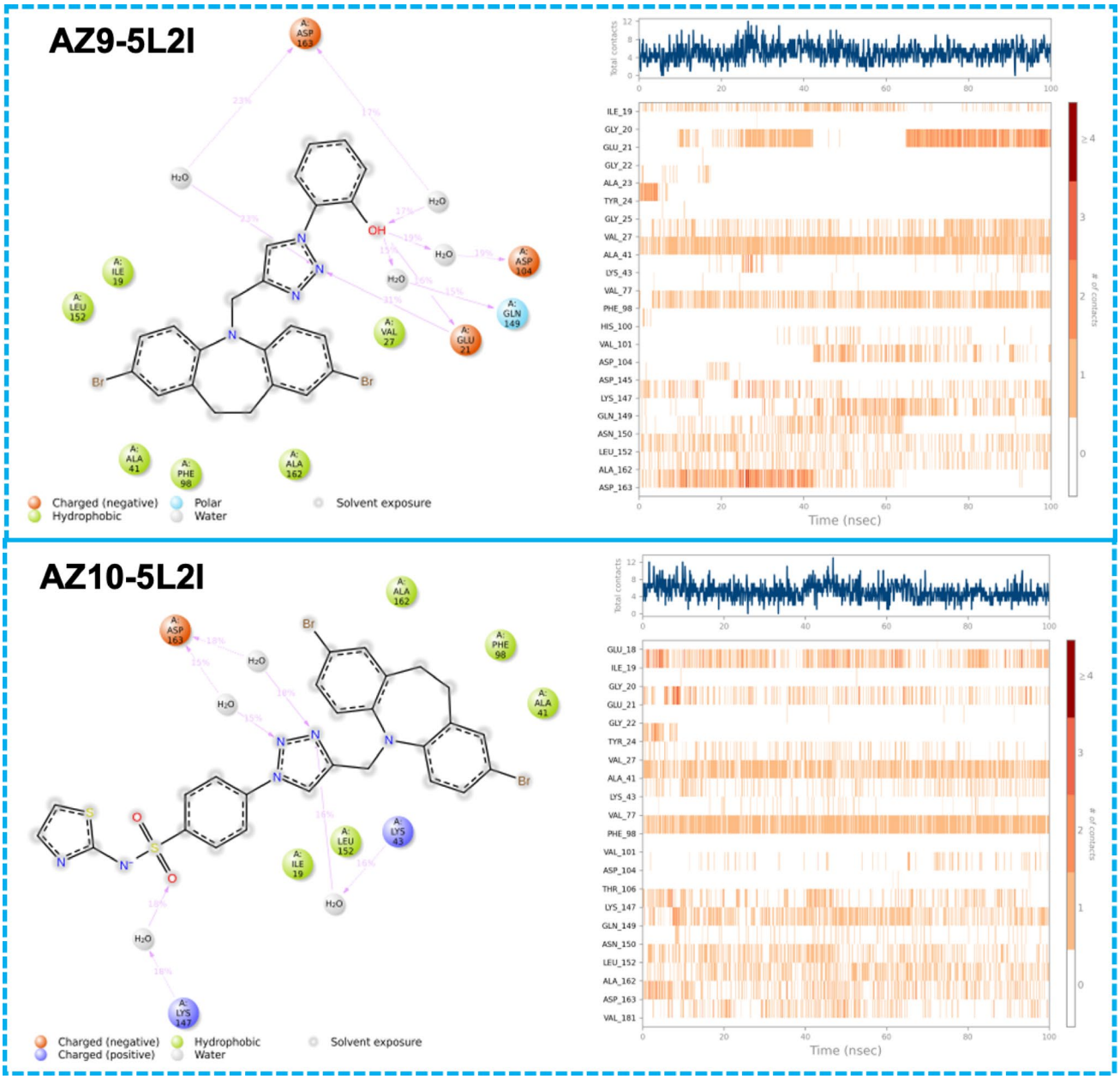

Fig. 6 (continued)

60 HF254 aluminium sheets. The conditions for spectroscopic analyses, including ^{1}H NMR, ^{13}C NMR, and mass spectrometry (Q-TOF-LC/MS), were described in our prior publication. In the NMR spectra, we reported coupling constants (*J* values) and chemical shifts (expressed in parts per million, ppm).

Preparation of the substituted Azide derivatives 1–10

The substituted azide derivatives **1–10** were prepared as in our previous study [32].

Synthesis of the compound 12

Under a nitrogen atmosphere, 4 g of silica gel was suspended in 75 mL of DCM in a two-neck 500 mL reaction flask at room temperature and stirred for 5 min. Subsequently, iminodibenzyl (**11**) (2 g, 10.24 mmol) was added to the reaction mixture. Then, a solution of NBS (3.65 g, 20.48 mmol) in a DCM : DMF (125:75, v/v, mL) mixture was added dropwise via a syringe. The reaction mixture was stirred at room temperature for 1 h. Upon completion, the mixture was filtered and extracted with DCM. The crude product was purified by column chromatography over 200 g of silica gel using 2–5%

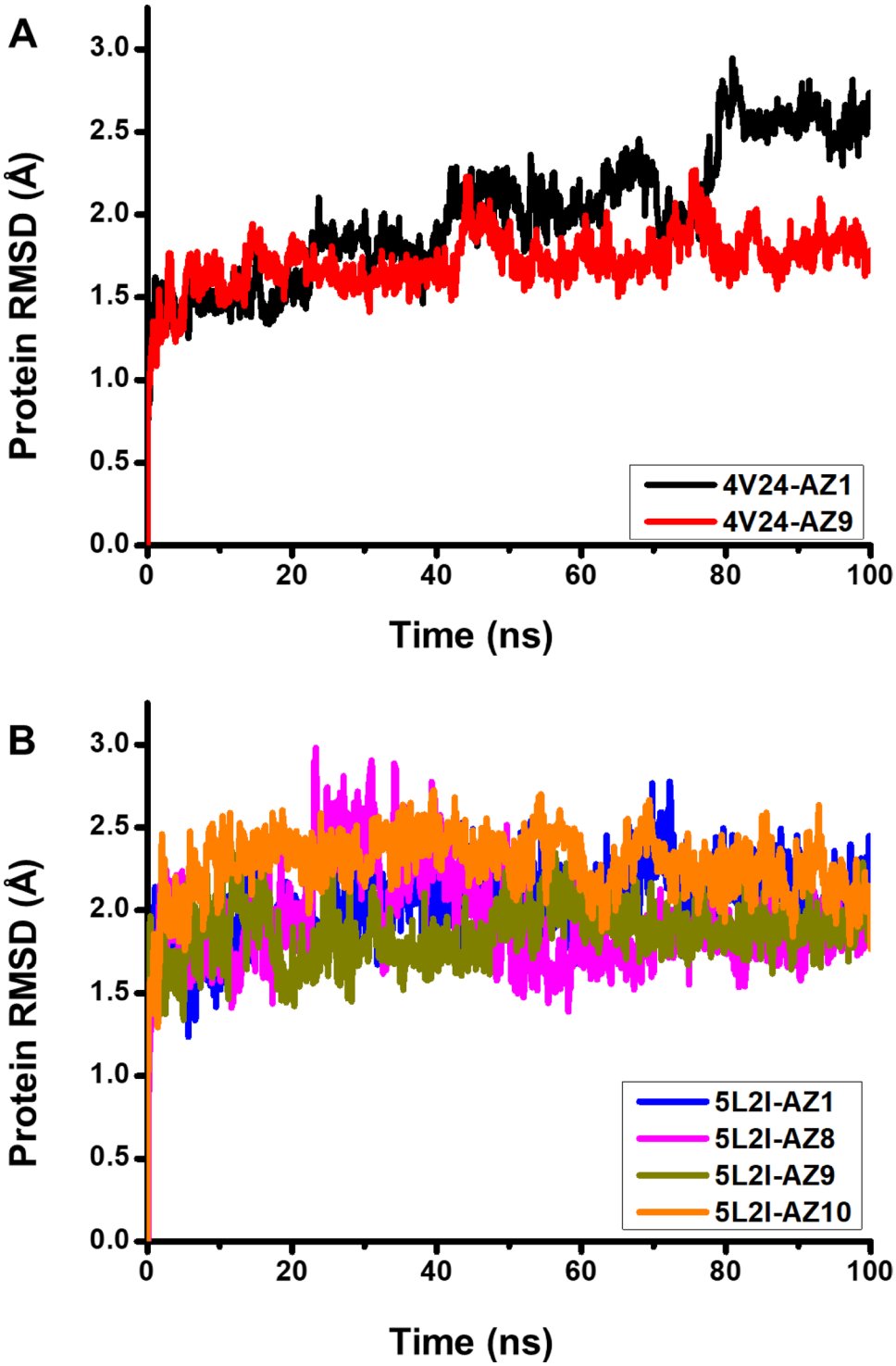

Fig. 7 The RMSD plot of the protein Cα for **A** SphK1-**AZ1** and SphK1-**AZ9** and **B** CDK6-**AZ1**, CDK6-**AZ8**, CDK6-**AZ9**, and CDK6-**AZ10**

Table 2 Binding free energy (ΔG_{bind}) calculations (MM/GBSA)

Targets	Compounds	Binding free energy (kcal/mol)
SphK1	**AZ1**	-79.76 ± 4.36
	AZ9	-84.06 ± 4.42
CDK6	**AZ1**	-61.57 ± 2.58
	AZ8	-71.06 ± 5.86
	AZ9	-69.38 ± 7.39
	AZ10	-83.52 ± 4.88

EtOAc in petroleum ether. The reaction afforded 3.40 g of dibromoazepine derivative **12** [47].

2,8-Dibromo-10,11-dihydro-5 H-dibenzo[b, f]azepine (12): White solids, 94%, mp 180–182 °C (lit.[37] mp 179–182 °C), ^{1}H NMR (400 MHz, $CDCl_3$) δ 7.26–7.11 (m, 4 H), 6.61 (s, 2 H), 5.96 (bs, 1H, -NH), 3.02 (s, 4 H). ^{13}C NMR (100

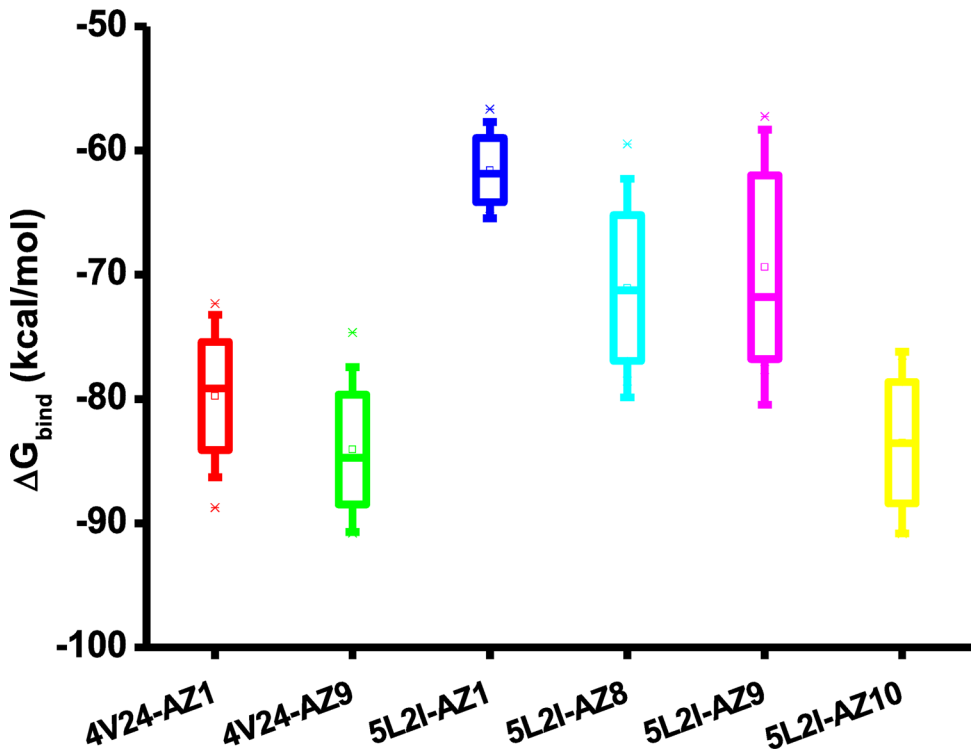

Fig. 8 Binding free energies (MM/GBSA)

Table 3 In Silico ADME analysis

Click products	[a]QPlogPw	[b]QPlogPo/w	[c]QPlogS	[d]QPPCaco	[e]QPlogBB	[f]QPlogHERG	[g]QPlogKhsa	[h]QPlogKp	[i]Human Oral Absorption	[j]Rule of Five
AZ1	6.216	6.945	-7.862	3795.606	0.270	-6.077	1.389	-0.705	1	2
AZ2	6.040	7.286	-8.970	3035.242	0.443	-6.176	1.580	-1.212	1	2
AZ3	7.718	5.784	-7.348	1693.324	0.014	-6.085	1.030	-1.648	1	2
AZ4	6.531	6.866	-8.400	3006.764	0.198	-6.198	1.438	-1.146	1	2
AZ5	6.799	7.759	-9.300	3392.759	0.318	-6.715	1.839	-0.737	1	1
AZ6	7.055	7.063	-8.660	3031.506	0.060	-5.962	1.416	-1.302	1	2
AZ7	7.404	6.031	-8.255	359.341	-0.813	-6.195	1.356	-2.957	1	2
AZ8	13.872	4.429	-7.448	142.837	-1.375	-6.363	0.761	-3.672	1	2
AZ9	8.333	6.149	-7.858	1272.921	-0.179	-6.097	1.289	-1.796	1	2
AZ10	10.769	6.618	-9.107	396.419	-0.899	-7.165	1.230	-2.400	1	2

[a]Predicted water/gas distribution coefficient: 4.0 − 45.0. [b]Predicted octanol/water distribution coefficient: −2.0 − 6.5. [c]Predicted aqueous solubility, logS. mol dm − 3 in S is the concentration of solute in a saturated solution in equilibrium with the crystalline solid: −6.5 − 0.5. [d]Estimated apparent Caco-2 cell permeability in nm/sec; Caco-2 cells are a model for the intestinal blood barrier; QikProp estimates are for inactive migration < 25 poor, >500 very good. [e]Predicted brain/blood distribution coefficient. Note: QikProp estimates are for oral medications, so dopamine and serotonin, for example, are CNS-negative because they are too polar to cross the very blood-brain barrier: −3.0 − 1.2. [f]Estimated IC50 value for blockade of HERG K + channels concern below − 5. [g]Prediction of binding to human serum albumin − 1.5 − 1.5. [h]Predicted skin permeability, log Kp: −8.0 to − 1.0. [i]Predicted qualitative human oral absorption: 1, 2, or 3 for low, medium, or high. [j]The number of violations of Lipinski's rule of five. The guidelines are mol MW < 500, QP log Po/w < 5, donorHB ≤ 5, acceptHB ≤ 10. Compounds meeting these guidelines are considered drug-like ("Five" means limits in multiples of 5) (maximum 4)

MHz, $CDCl_3$) δ 141.03, 133.11, 130.40, 129.67, 119.59, 111.74, 34.37.

Synthesis of propargyl derivative 13

Dibromoazepine derivative **12** (1.00 g, 2.83 mmol) was placed in a two-necked 200 mL round-bottom flask under a nitrogen atmosphere. The compound was dissolved in 10 mL of anhydrous DMF at 0 °C. Subsequently, KO*t*-Bu (0.60 g, 5.66 mmol) was added rapidly to the stirred solution, and the reaction mixture was maintained at 0 °C for 10 min. During this period, a distinct color change was observed as the solution turned green. After the initial stirring phase, propargyl bromide (1.5 mL, 17 mmol) was added dropwise

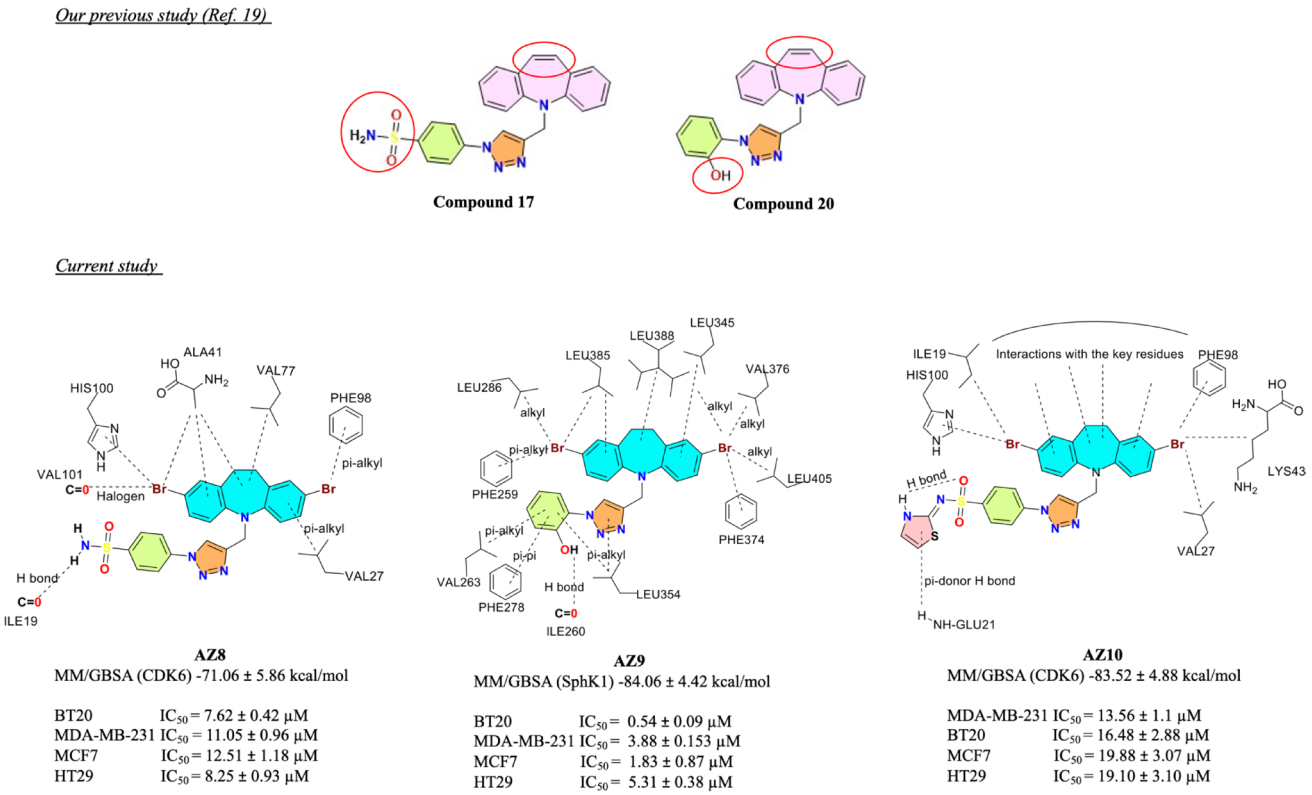

Fig. 9 A representation SAR for potential click products as anticancer agents

to the reaction mixture. The addition induced a further color change from green to brown, indicating progression of the reaction. The reaction's progress was monitored by TLC, and upon complete consumption of the starting material (after approximately 2 h), the reaction was quenched by the careful addition of ice-cold water. The resulting mixture was extracted with EtOAc (3 × 50 mL), and the combined organic extracts were dried over anhydrous Na_2SO_4. The solvent was then removed under reduced pressure using a rotary evaporator. The crude product was purified by column chromatography on 200 g of silica gel employing 10% EtOAc in petroleum ether as the eluent. This procedure afforded the dibromoazepine-propargyl derivative **13** (1.08 g). The product was characterized by ^{1}H NMR spectroscopy and used directly in the next reaction step.

2,8-Dibromo-5-(prop-2-yn-1-yl)-10,11-dihydro-5 H-dibenzo[b, f]azepine (**13**): Honey-like, 97%, ^{1}H NMR (400 MHz, $CDCl_3$) δ 7.29–7.26 (m, 4 H), 7.24 (s, 2 H), 4.38 (d, J = 2.4 Hz, 2 H), 3.09 (s, 4 H), 2.39 (t, J = 2.4 Hz, 1H). MS (MALDI-TOF): *m/z* calcd. for $C_{17}H_{13}Br_2N$ = 388.941 $[M]^+$; found: 389.356 $[M + H]^+$.

Synthesis and characterization of click products (AZ1-AZ10)

Dibromoazepine-propargyl derivative **13** (0.30 g, 1.0 mmol) was dissolved in a 45 mL mixture of THF/H_2O (2:1, v/v) at room temperature, along with the corresponding azide derivative (1.1 equiv.), (+) sodium *L*-ascorbate (0.3 equiv.), $CuSO_4$ (0.30 equiv.), and CuI (0.2 equiv.). To this mixture, 3–5 drops of NEt_3 were added, and the resulting solution was refluxed for 24 h. The formation of the desired products was monitored by TLC after 6–12 h. Once at least one of the starting materials was completely consumed, THF was removed under reduced pressure using a rotary evaporator. The crude product was extracted three times with 50 mL portions of EtOAc. The combined organic layers were dried over anhydrous Na_2SO_4, and the solvent was evaporated under reduced pressure. Finally, the crude product was purified by column chromatography on 200 g of silica gel. Spectroscopic analysis data for the click products are provided below.

Synthesis of 5-((1-benzyl-1 H-1,2,3-triazol-4-yl)methyl)-2,8-dibromo-10,11-dihydro-5 H-dibenzo[b, f]azepine (AZ1)

Cream solid, yield 99%, mp 147–149 °C, ^{1}H NMR (400 MHz, DMSO-d_6) δ 7.97 (s, 1H), 7.44–7.21 (m, 7 H), 7.15 (d, J = 8.6 Hz, 2 H), 7.03–6.85 (m, 2 H), 5.50 (s, 2 H), 4.96 (s, 2 H), 3.06 (s, 4 H). ^{13}C NMR (100 MHz, DMSO-d_6) δ 146.33, 144.13, 136.34, 136.26, 131.88, 128.90, 128.53, 127.76, 126.95, 124.22, 122.77, 114.67, 52.44, 46.61, 30.91. MS (MALDI-TOF): *m/z* calcd. for $C_{24}H_{20}Br_2N_4$ = 522.005 $[M]^+$; found: 522.990 $[M + H]^+$.

Synthesis of 2,8-Dibromo-5-((1-(4-chlorophenyl)-1 H-1,2,3-triazol-4-yl)methyl)-10,11-dihydro-5 H-dibenzo[b, f]azepine (AZ2)

Ivory solid, yield 95%, mp 95–97 °C, ^{1}H NMR (400 MHz, DMSO-d_6) δ 8.73 (s, 1H), 7.88 (d, J = 8.9 Hz, 2 H), 7.63 (d, J = 8.8 Hz, 2 H), 7.34–7.26 (m, 4 H), 7.24–7.18 (m, 2 H), 5.04 (s, 2 H), 3.12 (s, 4 H). ^{13}C NMR (100 MHz, DMSO-d_6) δ 146.49, 145.36, 136.33, 135.26, 132.79, 132.00, 129.80, 128.98, 122.62, 121.79, 121.46, 114.83, 46.46, 30.87. MS (MALDI-TOF): *m/z* calcd. for $C_{23}H_{17}Br_2ClN_4$ = 541.951 $[M]^+$; found: 542.326 $[M + H]^+$.

Synthesis of 2,8-Dibromo-5-((1-(pyridin-3-yl)-1 H-1,2,3-triazol-4-yl)methyl)-10,11-dihydro-5 H-dibenzo[b, f]azepine (AZ3)

Ivory solid, yield 90%, mp 202–204 °C, ^{1}H NMR (400 MHz, DMSO-d_6) δ 9.09 (d, J = 2.1 Hz, 1H), 8.81 (s, 1H), 8.66 (d, J = 4.6 Hz, 1H), 8.27 (d, J = 8.3 Hz, 1H), 7.61 (dd, J = 8.2, 4.8 Hz, 1H), 7.36–7.26 (m, 4 H), 7.26–7.23 (m, 2 H), 5.07 (s, 2 H), 3.13 (s, 4 H). ^{13}C NMR (100 MHz, DMSO-d_6) δ 149.56, 146.49, 145.50, 141.00, 136.35, 133.10, 132.01, 129.00, 127.59, 124.50, 122.61, 122.05, 114.85, 46.46, 30.88. MS (MALDI-TOF): *m/z* calcd. for $C_{22}H_{17}Br_2N_5$ = 508.985 $[M]^+$; found: 509.627 $[M + H]^+$.

Synthesis of 2,8-Dibromo-5-((1-(4-methoxyphenyl)-1 H-1,2,3-triazol-4-yl)methyl)-10,11-dihydro-5 H-dibenzo[b, f]azepine (AZ4)

Blush solid, yield 98%, mp 201–203 °C, ^{1}H NMR (400 MHz, DMSO-d_6) δ 8.58 (s, 1H), 7.73 (d, J = 9.0 Hz, 2 H), 7.35–7.25 (m, 4 H), 7.25–7.18 (m, 2 H), 7.09 (d, J = 9.0 Hz, 2 H), 5.02 (s, 2 H), 3.80 (s, 3 H), 3.12 (s, 4 H). ^{13}C NMR (100 MHz, DMSO-d_6) δ 159.15, 146.52, 144.89, 136.32, 131.97, 129.94, 128.96, 122.65, 121.62, 121.40, 114.84, 114.78, 55.55, 46.53, 30.89. MS (MALDI-TOF): *m/z* calcd. for $C_{24}H_{20}Br_2N_4O$ = 538.000 $[M]^+$; found: 538.497 $[M]^+$.

Synthesis of 2,8-Dibromo-5-((1-(naphthalen-1-yl)-1 H-1,2,3-triazol-4-yl)methyl)-10,11-dihydro-5 H-dibenzo[b, f]azepine (AZ5)

Colorless crystal, yield 89%, mp 233–235 °C, ^{1}H NMR (400 MHz, DMSO-d_6) δ 8.41 (s, 1H), 8.16 (d, J = 7.0 Hz, 1H), 8.09 (d, J = 8.2 Hz, 1H), 7.73–7.59 (m, 3 H), 7.50 (t, J = 7.7 Hz, 1H), 7.38–7.30 (m, 4 H), 7.27–7.22 (m, 2 H), 6.63 (d, J = 8.5 Hz, 1H), 5.13 (s, 2 H), 3.10 (s, 4 H). ^{13}C NMR (100 MHz, DMSO-d_6) δ 146.20, 144.09, 136.48, 133.54, 133.17, 131.92, 130.22, 128.95, 128.33, 128.15, 127.70, 127.02, 126.89, 125.40, 123.84, 122.94, 121.24, 114.75, 46.58, 30.93. MS (MALDI-TOF): *m/z* calcd. for $C_{27}H_{20}Br_2N_4$ = 558.005 $[M]^+$; found: 559.977 $[M + H]^+$.

Synthesis of 2,8-Dibromo-5-((1-(3,4,5-trimethoxyphenyl)-1 H-1,2,3-triazol-4-yl)methyl)-10,11-dihydro-5 H-dibenzo[b, f]azepine (AZ6)

White solid, yield 98%, mp 191–193 °C, ^{1}H NMR (400 MHz, DMSO-d_6) δ 8.74 (s, 1H), 7.34–7.27 (m, 4 H), 7.26–7.20 m, 2 H), 7.13 (d, J = 1.4 Hz, 2 H), 5.04 (s, 2 H), 3.85 (s, 6 H), 3.68 (s, 3 H), 3.12 (s, 4 H). ^{13}C NMR (100 MHz, DMSO-d_6) δ 153.49, 146.47, 144.91, 137.37, 136.30, 132.35, 131.97, 128.99, 122.69, 122.05, 114.79, 97.89, 60.18, 56.29, 46.51, 30.90. MS (MALDI-TOF): *m/z* calcd. for $C_{26}H_{24}Br_2N_4O_3$ = 598.022 $[M]^+$; found: 599.475 $[M + H]^+$.

Synthesis of 2,8-Dibromo-5-((1-(4-nitrophenyl)-1 H-1,2,3-triazol-4-yl)methyl)-10,11-dihydro-5 H-dibenzo[b, f]azepine (AZ7)

Light yellow solid, yield 87%, mp 217–219 °C, ^{1}H NMR (400 MHz, DMSO-d_6) δ 8.93 (s, 1H), 8.41 (d, J = 9.1 Hz, 2 H), 8.16 (d, J = 9.1 Hz, 2 H), 7.48–7.16 (m, 6 H), 5.08 (s, 2 H), 3.13 (s, 4 H). ^{13}C NMR (100 MHz, DMSO-d_6) δ 146.60, 146.43, 145.87, 140.68, 136.34, 132.02, 129.00, 125.51, 122.60, 122.24, 120.36, 114.88, 46.39, 30.87. MS (MALDI-TOF): *m/z* calcd. for $C_{23}H_{17}Br_2N_5O_2$ = 552.975 $[M]^+$; found: 552.700 $[M]^+$.

Synthesis of 4-(4-((2,8-dibromo-10,11-dihydro-5 H-dibenzo[b, f]azepin-5-yl)methyl)-1 H-1,2,3-triazol-1-yl)benzenesulfonamide (AZ8)

Bronze solid, yield 74%, mp 257–259 °C, ^{1}H NMR (400 MHz, DMSO-d_6) δ 8.81 (s, 1H), 8.06 (d, J = 8.7 Hz, 2 H), 7.98 (d, J = 8.7 Hz, 2 H), 7.53 (s, 2 H, -NH_2), 7.35–7.19 (m, 6 H), 5.07 (s, 2 H), 3.13 (s, 4 H). ^{13}C NMR (100 MHz, DMSO-d_6) δ 146.48, 145.55, 143.76, 138.43, 136.34, 132.01, 129.00, 127.44, 122.62, 122.01, 120.05, 114.86,

46.43, 30.89. MS (MALDI-TOF): *m/z* calcd. for $C_{23}H_{19}Br_2N_5O_2S$ = 586.963 $[M]^+$; found: 587.087 $[M + H]^+$.

Synthesis of 2-(4-((2,8-dibromo-10,11-dihydro-5 H-dibenzo[b, f]azepin-5-yl)methyl)-1 H-1,2,3-triazol-1-yl)phenol (AZ9)

Bronze solid, yield 75%, mp 194–196 °C, ^{1}H NMR (400 MHz, DMSO-d_6) δ 10.51 (s, 1H, -OH), 8.31 (s, 1H), 7.54 (dd, *J* = 7.9, 1.3 Hz, 1H), 7.36–7.20 (m, 7 H), 7.06 (dd, *J* = 8.2, 0.9 Hz, 1H), 6.94 (t, *J* = 7.6 Hz, 1H), 5.04 (s, 2 H), 3.09 (s, 4 H). ^{13}C NMR (100 MHz, DMSO-d_6) δ 149.13, 146.60, 143.62, 136.26, 131.95, 129.84, 128.98, 125.04, 124.56, 124.39, 122.73, 119.52, 117.07, 114.74, 46.44, 30.89. MS (MALDI-TOF): *m/z* calcd. for $C_{23}H_{18}Br_2N_4O$ = 523.985 $[M]^+$; found: 524.969 $[M + H]^+$.

Synthesis of 4-(4-((2,8-dibromo-10,11-dihydro-5 H-dibenzo[b, f]azepin-5-yl)methyl)-1 H-1,2,3-triazol-1-yl)-N-(thiazol-2-yl)benzenesulfonamide (AZ10)

Soil solid, yield 72%, mp 150–152 °C, ^{1}H NMR (400 MHz, DMSO-d_6) δ 12.87 (bs, 1H), 8.78 (s, 1H), 8.12–7.82 (m, 4 H), 7.36–7.14 (m, 7 H), 6.87 (bs, 1H), 5.05 (s, 2 H), 3.12 (s, 4 H). ^{13}C NMR spectrum of the compound could not be obtained due to poor resolution. MS (MALDI-TOF): *m/z* calcd. for $C_{26}H_{20}Br_2N_6O_2S_2$ = 669.946 $[M]^+$; found: 669.807 $[M]^+$.

Cell culture conditions and cytotoxicity assay

Various human cancer cell lines were used in this study. TNBC (MDA-MB-231 and BT20), estrogen receptor positive (ER+), and colon (HT29) cell lines were gift. The cells were cultured in DMEM/F12, 10% FBS, and 1% PS, and incubated under 5% CO_2 in an incubator. The cytotoxicity of the synthesized compounds was determined by MTT ((3-(4,5-dimethylthiazol-2-yl)-2,5-diphenyltetrazolium bromide)) method according to our reported studies [19, 36, 48, 49]. The cells were treated with the compounds in the increasing concentrations for 96 h. The absorbances of the compounds were measured at 570 nm.

Computational analysis

Molecular docking

The protein-ligand interaction analysis of the synthesized compounds against significant cancer drug targets including sphingosine kinase 1 (SphK1) and cell division protein kinase 6 (CDK6) was assessed using the Glide/SP [50]. The protein crystal structures (PDBs: 4V24 and 5L2I) were downloaded from Protein Data Bank (https://www.rcsb.org/). Proteins and ligands were prepared using Protein Preparation Wizard and LigPrep [51] by using OPLS4 force field [52]. Co-crystallized ligands of the proteins were used to generate grid box by Receptor Grid Generation (Maestro, Schrödinger, LLC). The 2D ligand interactions were visualized by BIOVIA Discovery Studio (DS).

MD simulation and MM/GBSA analysis

Desmond [53] and Prime [54] methods were used to conduct MD simulations and MM/GBSA analysis, respectively. MD simulations were performed using top docking poses of each compound. Based on the obtained results, binding free energies (ΔG_{bind}) were calculated as kcal/mol using 10-ns trajectories for each complex [55, 56].

ADME analysis

Qikprop was used for in silico ADME predictions according to the reported studies [19, 36]. This method estimates optimum ranges for 95% of known drugs [41].

Supplementary Information The online version contains supplementary material available at https://doi.org/10.1007/s11030-025-11418-w.

Acknowledgements The authors are grateful to Prof. Dr. Zuhal Hamurcu (Erciyes University) and Prof. Dr. Tuğba Tümer (Çanakkale Onsekiz Mart University) for providing breast and colon cancer cell lines. This research has been supported by the Kafkas University Scientific Research Projects Coordination Unit (Project Number: 2023-FM-105). The authors are grateful to the Research Foundation of Kafkas University for financial support under project 2023-FM-105.

Author contributions Musa Erdoğan designed the project; Azza Allıto and Musa Erdoğan synthesized and characterized the compounds; Alper Onder performed the in silico studies; Ferah Comert Onder performed the anticancer assays; Musa Erdoğan and Ferah Comert Onder wrote the initial draft of the manuscript, revised it, and approved the final version.

Data availability The data was given in supporting information.

Declarations

Conflict of interest The authors state no conflict of interest.

References

1. Siegel RL, Kratzer TB, Giaquinto AN et al (2025) Cancer statistics, 2025. CA Cancer J Clin 75:10–45. https://doi.org/10.3322/caac.21871

2. Pucci C, Martinelli C, Ciofani G (2019) Innovative approaches for cancer treatment: current perspectives and new challenges. ecancer 13:961. https://doi.org/10.3332/ecancer.2019.961
3. Housman G, Byler S, Heerboth S et al (2014) Drug resistance in cancer: an overview. Cancers 6:1769–1792. https://doi.org/10.3390/cancers6031769
4. Pourgholi A, Dadashpour M, Mousapour A et al (2021) Anticancer potential of Silibinin loaded polymeric nanoparticles against breast cancer cells: insight into the apoptotic genes targets. Asian Pac J Cancer Prev 22:2587–2596. https://doi.org/10.31557/APJCP.2021.22.8.2587
5. Doostmohammadi A, Jooya H, Ghorbanian K et al (2024) Potentials and future perspectives of multi-target drugs in cancer treatment: the next generation anti-cancer agents. Cell Commun Signal 22:228. https://doi.org/10.1186/s12964-024-01607-9
6. Bray F, Laversanne M, Sung H et al (2024) Global cancer statistics 2022: GLOBOCAN estimates of incidence and mortality worldwide for 36 cancers in 185 countries. CA Cancer J Clin 74:229–263. https://doi.org/10.3322/caac.21834
7. Gadakh S, Aghav B, Teraiya N et al (2025) Discovery of novel Benzoxazole analogues as potential anticancer agent selectively targeting aromatase. Bioorg Med Chem 122:118142. https://doi.org/10.1016/j.bmc.2025.118142
8. Hoelder S, Clarke PA, Workman P (2012) Discovery of small molecule cancer drugs: successes, challenges and opportunities. Mol Oncol 6:155–176. https://doi.org/10.1016/j.molonc.2012.02.004
9. Cui W, Aouidate A, Wang S et al (2020) Discovering anti-cancer drugs via computational methods. Front Pharmacol 11:733. https://doi.org/10.3389/fphar.2020.00733
10. Kairys V, Baranauskiene L, Kazlauskiene M et al (2019) Binding affinity in drug design: experimental and computational techniques. Expert Opin Drug Discov 14:755–768. https://doi.org/10.1080/17460441.2019.1623202
11. Zhang S, Liu K, Liu Y et al (2025) The role and application of bioinformatics techniques and tools in drug discovery. Front Pharmacol 16:1547131. https://doi.org/10.3389/fphar.2025.1547131
12. Wu G, Zhao T, Kang D et al (2019) Overview of recent strategic advances in medicinal chemistry. J Med Chem 62:9375–9414. https://doi.org/10.1021/acs.jmedchem.9b00359
13. Mermer A, Keles T, Sirin Y (2021) Recent studies of nitrogen containing heterocyclic compounds as novel antiviral agents: a review. Bioorg Chem 114:105076. https://doi.org/10.1016/j.bioorg.2021.105076
14. Kassem AF, Moustafa GO, Omran MM, El-Sofany WI (2024) Investigation on the Pharmacological profile for new synthesized Bis heterocyclic analogs containing nitrogen atom as anti-cancer therapy target. J Mol Struct 1312:138450. https://doi.org/10.1016/j.molstruc.2024.138450
15. Behl C, Moosmann B (2002) Antioxidant neuroprotection in alzheimer's disease as preventive and therapeutic approach. This article is part of a series of reviews on "Causes and Consequences of Oxidative Stress in Alzheimer's Disease." The full list of papers may be found on the homepage of the journal. Free Radic Biol Med 33:182–191. https://doi.org/10.1016/S0891-5849(02)00883-3
16. Erdoğan M, Daştan A (2020) Synthesis of N -substituted dibenzoazepine–pyridazine derivatives as potential neurologically active drugs. Synth Commun 50:3845–3853. https://doi.org/10.1080/00397911.2020.1828925
17. Landek IO, Pešić D, Merćep M et al (2011) Synthesis and anti-inflammatory activity of 8H-1-thia-8-aza-dibenzo[e,h]azulenes. J Heterocycl Chem 48:856–863. https://doi.org/10.1002/jhet.605
18. Sadashiva MP, Basappa, NanjundaSwamy S et al (2012) Anticancer activity of novel dibenzo[b,f]azepine tethered isoxazoline derivatives. BMC Chem Biol 12:5. https://doi.org/10.1186/1472-6769-12-5
19. Erdoğan M, Onder A, Demir Y, Comert Onder F (2024) Novel Dibenzoazepine-Substituted Triazole hybrids as cholinesterase and carbonic anhydrase inhibitors and anticancer agents: synthesis, Characterization, biological Evaluation, and in Silico studies. ACS Omega 9:46860–46878. https://doi.org/10.1021/acsomega.4c05804
20. Shah H, Pang L, Qian S, Sathish V (2021) Iminodibenzyl induced redirected COX-2 activity inhibits breast cancer progression. npj Breast Cancer 7:122. https://doi.org/10.1038/s41523-021-00330-9
21. Alam MM (2022) 1,2,3-Triazole hybrids as anticancer agents: a review. Arch Pharm 355:2100158. https://doi.org/10.1002/ardp.202100158
22. Bozorov K, Zhao J, Aisa HA (2019) 1,2,3-Triazole-containing hybrids as leads in medicinal chemistry: a recent overview. Bioorg Med Chem 27:3511–3531. https://doi.org/10.1016/j.bmc.2019.07.005
23. Zhao S, Liu J, Lv Z et al (2023) Recent updates on 1,2,3-triazole-containing hybrids with in vivo therapeutic potential against cancers: a mini-review. Eur J Med Chem 251:115254. https://doi.org/10.1016/j.ejmech.2023.115254
24. Vaishnani MJ, Bijani S, Rahamathulla M et al (2024) Biological importance and synthesis of 1,2,3-triazole derivatives: a review. Green Chem Lett Rev 17:2307989. https://doi.org/10.1080/17518253.2024.2307989
25. Salma U, Ahmad S, Md ZA, Khan SA (2024) A review: synthetic approaches and biological applications of Triazole derivatives. J Mol Struct 1301:137240. https://doi.org/10.1016/j.molstruc.2023.137240
26. Kumar S, Sharma B, Mehra V, Kumar V (2021) Recent accomplishments on the synthetic/biological facets of pharmacologically active 1H-1,2,3-triazoles. Eur J Med Chem 212:113069. https://doi.org/10.1016/j.ejmech.2020.113069
27. Arun B, Brahmayya M, Sreenivasulu R et al (2025) Rational design and synthesis of 1,2,3-Triazole incorporated Oxazolo[5,4-d] pyrimidine derivatives: in-vitro cytotoxicity and In-Silico molecular Docking simulations. Polycycl Aromat Compd 45:1515–1535. https://doi.org/10.1080/10406638.2025.2467956
28. Shahinshavali S, Poojith N, Guttikonda VR et al (2020) Design, synthesis and anticancer evaluation of acetamides comprising 1,2,3-triazole, 1,3,4-thiadiazole and Isothiazolo[4,3-b]pyridine rings. LOC 17:864–871. https://doi.org/10.2174/1570178617666200225102939
29. Murthy IS, Sreenivasulu R, Alluraiah G, Ramesh Raju R (2019) Design, synthesis, and anticancer activity of 1,2,3-Triazole linked 1,2-Isoxazole-imidazo[4,5-b]pyridine derivatives. Russ J Gen Chem 89:1718–1723. https://doi.org/10.1134/S1070363219080279
30. Yakantham T, Sreenivasulu R, Alluraiah G et al (2019) Design, synthesis, and anticancer activity of 1,2,3-Triazole likned Thiazole-1,2-isoxazole derivatives. Russ J Gen Chem 89:2522–2527. https://doi.org/10.1134/S1070363219120314
31. Allıto L, Comert Onder F, Demirel R et al (2025) Design, synthesis, characterization, in Silico studies, and in vitro anticancer evaluation of novel 7-methoxyquinolone-substituted Triazole hybrids. Future Med Chem 17:1559–1573. https://doi.org/10.1080/17568919.2025.2533003
32. Ngameni B, Erdoğan M, Kuete V et al (2021) Synthesis and structural characterization of novel O -substituted phenolic and chalcone derivatives with antioxidant activity. J Chem Res 45:159–165. https://doi.org/10.1177/1747519820932789
33. Yuan K, Wang X, Dong H et al (2021) Selective Inhibition of CDK4/6: a safe and effective strategy for developing anticancer

drugs. Acta Pharm Sin B 11:30–54. https://doi.org/10.1016/j.apsb.2020.05.001
34. Siemeister G, Lücking U, Wengner AM et al (2012) BAY 1000394, a novel cyclin-dependent kinase Inhibitor, with potent antitumor activity in Mono- and in combination treatment upon oral application. Mol Cancer Ther 11:2265–2273. https://doi.org/10.1158/1535-7163.MCT-12-0286
35. Byth KF, Thomas A, Hughes G et al (2009) AZD5438, a potent oral inhibitor of cyclin-dependent kinases 1, 2, and 9, leads to pharmacodynamic changes and potent antitumor effects in human tumor xenografts. Mol Cancer Ther 8:1856–1866. https://doi.org/10.1158/1535-7163.MCT-08-0836
36. Erdoğan M, Comert Onder F (2024) Synthesis, anticancer activity and molecular modeling study of novel substituted Triazole linked tetrafluoronaphthalene hybrid derivatives. J Biomol Struct Dyn 42:9767–9786. https://doi.org/10.1080/07391102.2023.2252914
37. Jairajpuri DS, Mohammad T, Adhikari K et al (2020) Identification of sphingosine Kinase-1 inhibitors from bioactive natural products targeting cancer therapy. ACS Omega 5:14720–14729. https://doi.org/10.1021/acsomega.0c01511
38. Khan FI, Lai D, Anwer R et al (2020) Identifying novel sphingosine kinase 1 inhibitors as therapeutics against breast cancer. J Enzyme Inhib Med Chem 35:172–186. https://doi.org/10.1080/14756366.2019.1692828
39. Önder A, Davutlar G, Ay M, Cömert Önder F (2024) Virtual Screening, molecular Docking, and molecular dynamics simulation studies on potential phytochemicals as sphingosine kinase 1 inhibitors for cancer therapy. Int J Life Sci Biotechnol. https://doi.org/10.38001/ijlsb.1444789
40. Kruschel RD, Malone K, Walsh AN et al (2025) Discovery of sphingosine kinase Inhibition by modified Quinoline-5,8-Diones. Pharmaceuticals 18:268. https://doi.org/10.3390/ph18020268
41. Ntie-Kang F, Lifongo LL, Mbah JA et al (2013) In Silico drug metabolism and pharmacokinetic profiles of natural products from medicinal plants in the congo basin. Silico Pharmacol 1:12. https://doi.org/10.1186/2193-9616-1-12
42. Amengor CDK, Orman E, Danquah CA et al (2022) Pyridine-N-Oxide alkaloids from allium stipitatum and their synthetic disulfide analogs as potential drug candidates against *Mycobacterium tuberculosis*: a molecular docking, QSBAR, and ADMET prediction approach. Biomed Res Int 2022:6261528. https://doi.org/10.1155/2022/6261528
43. Demir Y, Şenol H, Uluçay O et al (2026) Morpholine-modified thiosemicarbazones and thiazolidin-4-ones against Alzheimer's key enzymes: from synthesis to Inhibition. Comput Biol Chem 120:108683. https://doi.org/10.1016/j.compbiolchem.2025.108683
44. Jana S, Mandlekar S, Marathe P (2010) Prodrug design to improve Pharmacokinetic and drug delivery properties: challenges to the discovery scientists. CMC 17:3874–3908. https://doi.org/10.2174/092986710793205426
45. Savla R, Browne J, Plassat V et al (2017) Review and analysis of FDA approved drugs using lipid-based formulations. Drug Dev Ind Pharm 43:1743–1758. https://doi.org/10.1080/03639045.2017.1342654
46. Gupta S, Kesarla R, Omri A (2013) Formulation strategies to improve the bioavailability of poorly absorbed drugs with special emphasis on self-emulsifying systems. ISRN Pharm 2013:1–16. https://doi.org/10.1155/2013/848043
47. Basak S, Alvarez-Montoya A, Winfrey L et al (2020) B(C6 F5)3-catalyzed direct C3 alkylation of Indoles and oxindoles. ACS Catal 10:4835–4840. https://doi.org/10.1021/acscatal.0c01141
48. Comert Onder F, Ural K, Onder A et al (2025) New and potential boron-containing compounds for treatment of Alzheimer's disease and cancers. Future Med Chem 17:1377–1389. https://doi.org/10.1080/17568919.2025.2525065
49. Abusharkh KAN, Comert Onder F, Çınar V et al (2024) A drug repurposing study identifies novel FOXM1 inhibitors with in vitro activity against breast cancer cells. Med Oncol 41:188. https://doi.org/10.1007/s12032-024-02427-0
50. Friesner RA, Murphy RB, Repasky MP et al (2006) Extra precision glide: docking and scoring incorporating a model of hydrophobic enclosure for protein –ligand complexes. J Med Chem 49:6177–6196. https://doi.org/10.1021/jm051256o
51. Madhavi Sastry G, Adzhigirey M, Day T et al (2013) Protein and ligand preparation: parameters, protocols, and influence on virtual screening enrichments. J Comput Aided Mol Des 27:221–234. https://doi.org/10.1007/s10822-013-9644-8
52. Jorgensen WL, Maxwell DS, Tirado-Rives J (1996) Development and testing of the OPLS All-Atom force field on conformational energetics and properties of organic liquids. J Am Chem Soc 118:11225–11236. https://doi.org/10.1021/ja9621760
53. Bowers KJ, Sacerdoti FD, Salmon JK et al (2006) Molecular dynamics—Scalable algorithms for molecular dynamics simulations on commodity clusters. In: Proceedings of the 2006 ACM/IEEE conference on supercomputing - SC '06. ACM Press, Tampa, p 84
54. Jacobson MP, Pincus DL, Rapp CS et al (2004) A hierarchical approach to all-atom protein loop prediction. Proteins 55:351–367. https://doi.org/10.1002/prot.10613
55. Kalin S, Comert Onder F (2025) Discovery of potential RSK1 inhibitors for cancer therapy using virtual screening, molecular docking, molecular dynamics simulation, and MM/GBSA calculations. J Biomol Struct Dyn 43:1424–1444. https://doi.org/10.1080/07391102.2023.2291830
56. Comert Onder F, Ural K, Onder A et al (2025) Boron containing Curcumin-Like compound as an acetylcholinesterase inhibitor and anticancer agent: synthesis, biological evaluation, and computational insights. Cell Biochem Biophys. https://doi.org/10.1007/s12013-025-01885-1

Publisher's note Springer Nature remains neutral with regard to jurisdictional claims in published maps and institutional affiliations.

Springer Nature or its licensor (e.g. a society or other partner) holds exclusive rights to this article under a publishing agreement with the author(s) or other rightsholder(s); author self-archiving of the accepted manuscript version of this article is solely governed by the terms of such publishing agreement and applicable law.